

MOL 14068

Integration of Virtual Screening With High Throughput Flow Cytometry to Identify Novel Small Molecule Formylpeptide Receptor Antagonists

Bruce S. Edwards, Cristian Bologa, Susan M. Young, Konstantin V. Balakin, Eric R. Prossnitz, Nikolay P. Savchuck, Larry A. Sklar, Tudor I. Oprea

Cytometry (BSE,SMY,LAS), Biocomputing (CB,TIO), Pathology (BSE,LAS), Cell Biology and Physiology (ERP), University of New Mexico Health Sciences Center, Albuquerque, NM; and Chemical Diversity Laboratories, Inc., San Diego, CA (KVB,NPS)

MOL 14068

Running Title: Integrating Virtual and Flow Cytometry Screening

Corresponding author: Tudor I. Oprea, Division of Biocomputing, MSC11 6145, Research Incubator Building S-te 190, UNM HSC, 1 University of New Mexico, Albuquerque NM 87131-0001; E-mail: T_Oprea@salud.unm.edu ; Phone, 505-272-3694; Fax, 505-272- 8738.

Number of text pages:	24
Number of tables:	1
Number of figures:	5
Number of supplemental figures:	2
Number of references:	40
Number of words in Abstract:	159
Number of words in Introduction:	578
Number of words in Discussion:	719

Abbreviations: 4Pep, formylmethionine-leucine-phenylalanine-phenylalanine or fMLFF; FPR, formylpeptide receptor; GPCR, G protein-coupled receptor; HTFC, high-throughput flow cytometry; IC₅₀, concentration resulting in 50% inhibition; K_i, inhibition constant; LBVS, ligand-based virtual screening; MFI, median fluorescence intensity.

MOL 14068

Abstract

The formylpeptide receptor (FPR) family of G-protein coupled receptors (GPCR) contributes to the localization and activation of tissue-damaging leukocytes at sites of chronic inflammation. We developed a FPR homology model and pharmacophore (based on the bovine rhodopsin crystal structure and known FPR ligands, respectively) for *in silico* screening of ~480,000 drug-like small molecules. A subset of 4,324 compounds that matched the pharmacophore was then physically screened with the HyperCyt[®] flow cytometry platform in high-throughput no-wash assays that directly measure human FPR binding, with samples (each ~ 2,500 cells in 2 μ L) analyzed at 40/min. From 52 confirmed hits (1.2% hit rate) we identified 30 potential lead compounds (inhibition constant, K_i = 1-32 μ M) representing 9 distinct chemical families. Four compounds in one family were weak partial agonists. All others were antagonists. This virtual screening approach improved the physical screening hit rate 12-fold (vs. 0.1% hit-rate in a random compound collection), providing an efficient process for identifying small molecule antagonists.

MOL 14068

Introduction

The G-protein coupled formylpeptide receptor (FPR) was one of the originating members of the chemoattractant receptor superfamily (Le et al., 2002; Oppenheim et al., 1991). N-formylated peptides such as fMLF are high affinity FPR ligands that trigger a variety of biologic activities in myeloid cells, including chemokinesis, chemotaxis, cytokine production and superoxide generation (He et al., 2003; Le et al., 2001; Murphy, 1994; Tiffany et al., 2001). Since such peptides are derived from bacterial or mitochondrial proteins (Carp, 1982; Marasco et al., 1984; Schiffmann et al., 1975), it has been proposed that a primary FPR function is to promote trafficking of phagocytic myeloid cells to sites of infection and tissue damage where they exert anti-bacterial effector functions and clear cell debris. In support of this hypothesis, mice lacking a known murine FPR variant were more susceptible to bacterial infections (Gao et al., 1999). Long known to be expressed by neutrophils and monocytes, FPR have more recently been identified in hepatocytes, immature dendritic cells, astrocytes, microglial cells, and the tunica media of coronary arteries (Le et al., 2002). The glucocorticoid-regulated protein, annexin I (lipocortin I), was recently identified as a protein of host origin that is a specific agonist for human FPR (Walther et al., 2000). Moreover, HIV-1 envelope proteins contain domains capable of interacting with either or both FPR and the related FPR family member, FPRL1 (Le et al., 2000; Su et al., 1999; VanCompernelle et al., 2003). These receptors have been proposed as prospective targets for therapeutic intervention against malignant gliomas (<http://pharmalicensing.com/licensing/displcopp/3019>). The diverse tissue expression of FPR and the expanding range of identified FPR ligands suggest the possibility of as yet unappreciated complexity in the innate immune response and perhaps other unidentified physiological functions for FPR.

HyperCyt[®] is a novel automated high throughput flow cytometry (HTFC) analysis platform by which cell samples are rapidly aspirated from microplate wells and delivered to the flow cytometer. Accurate quantitative measurements have been

MOL 14068

demonstrated in endpoint assays at 40 samples/min over a 4-decade range of fluorescence intensity. Intact cells may be used at concentrations of 1–20 million/ml in assay volumes of 8-15 μ l (Ramirez et al., 2003). Typical sample volumes of 1-2 μ l from each assay volume allow scarce quantities of test cells or reagents to be efficiently utilized. We recently initiated a HyperCyt[®]-based HTFC screening effort to detect potential anti-inflammatory compounds that block ligand binding to FPR. A fluorescence-based HTFC ligand competition assay was characterized and validated in screening of the Prestwick Chemical Library (Young et al., 2005). A previously documented FPR antagonist with an inhibition constant (K_i) of ~14 μ M was detected from among the 880 small molecule drugs and alkaloids screened (Young et al., 2005).

The present study was subsequently undertaken to identify novel small molecule FPR ligands. We first developed a computational FPR model that employed a homology model of rhodopsin, the only vertebrate GPCR crystallized to date, together with a pharmacophore model constructed on the basis of previously documented FPR agonists and antagonists. The computational model was then used to screen a commercial collection of ~480,000 compounds *in silico*, identifying a small subset predicted to be enriched with FPR antagonists. Supporting this prediction, and the hypotheses underpinning the model, the frequency of active structures detected in subsequent HTFC screening was more than 10-fold higher than expected from a random compound collection. We identified potential lead structures representing 9 distinct chemical families, a group of promising reagents for probing FPR functional diversity and therapeutic significance.

MOL 14068

Materials and Methods

Compounds. The Chemical Diversity Laboratories collection (~480,000 compounds) was filtered (Olah et al., 2004) for molecular weight (range 150–600) and atom type content (only C, N, O, H, S, P, F, Cl, Br, and I were permitted). A 3D pharmacophore hypothesis was then used for the virtual screening of the remaining collection of 434,000 structures (see below). Based on this model, 4,234 structures with the proper 3D arrangement of topological elements matching the pharmacophore were made available for physical screening at UNM.

Cells and reagents. Fluorescein-labeled formylmethionine-leucine-phenylalanine-lysine (fMLFK-FITC) and unlabeled formylmethionine-leucine-phenylalanine-phenylalanine (fMLFF, 4PeP), formylmethionine-leucine (fML, 2Pep) and formylnorleucine-leucine-phenylalanine-norleucine-tyrosine-lysine (fNleLFNleYK) were obtained from Peninsula Labs (San Carlos, CA). The fNleLFNleYK was tagged with Alexa-633 (Molecular Probes, Eugene, OR) as previously described (Key et al., 2003). Myeloid U937 cells transfected with the human FPR were cultured in RPMI-1640 medium supplemented with 10% fetal bovine serum (Hyclone), 2mM L-glutamine, 10 mM HEPES, 10U/ml penicillin and 10 µg/ml streptomycin, 4 µg/ml CIPRO, and 500 µg/ml Geneticin (Invitrogen, Japan). Cultures were grown at 37° C in a 5% CO₂ atmosphere, and passaged every three days. Unless otherwise indicated, U937 cells were used that expressed a mutant FPR with glycine and alanine substituted for serine and threonine residues in the C-terminal tail (DeltaST) (Prossnitz, 1997). DeltaST cells do not internalize the receptor when stimulated with fMLF (Prossnitz, 1997). Chemical reagents were obtained from Sigma (St. Louis, MO) unless otherwise specified. Mouse melanoma B78H1 cells expressing the transfected human VCAM-1 gene (B78H1-VCAM1) were prepared and cultured as previously described (Chigae, 2003).

MOL 14068

FPR assay. The FPR assay measured the ability of test compounds to compete with a high-affinity fluorescent ligand, fMLFK-FITC, for binding to cell membrane FPR. The assay has recently been characterized and validated in a separate series of studies (Young et al., 2005). The assay response range was defined by replicate control wells containing unlabeled fMLFF blocking peptide (4Pep) or buffer alone. Unlabeled fMLFF was at a 100-fold higher concentration that completely blocked binding of the fluorescent ligand, hence wells containing this were designated blocked controls. Control wells containing buffer alone were designated unblocked controls. Test compound inhibition of fluorescent peptide binding was calculated as $100 \times [1 - (MFI_{\text{Test}} - MFI_{\text{Blocked}})/(MFI_{\text{Unblocked}} - MFI_{\text{Blocked}})]$, in which MFI was the median fluorescence intensity of cells in wells containing test compounds, blocked control wells and unblocked control wells as indicated by subscripts of each MFI term in the equation. Compounds inhibiting 70% or more were considered 'hits'.

For assay performance, additions to wells were in sequence as follows: 1st, test compounds and control reagents (5 μ l/well); 2nd, cells (10^7 /ml, 5 μ l/well); 3rd, (after 30 min, 4°C incubation) fMLFK-FITC (5 μ l/well). After an additional 45 min, 4°C incubation, plates were immediately analyzed by flow cytometry with the HyperCyt[®] platform.

MFI measurements from control wells were also used to calculate a Z' factor for each assay. The Z' factor is a measure of screening assay quality that reflects both assay signal dynamic range and data variation associated with the signal measurements (Zhang et al., 1999). The Z' factor for 268 plates analyzed in this and other studies was 0.62 ± 0.16 (mean \pm SD)

Chemical Diversity Laboratories compounds were provided as 10 mM stock solutions in DMSO and were diluted in assay dilution buffer (ADB; 110 mM NaCl, 30 mM HEPES, 10 mM KCl, 1mM MgCl₂, 10 mM glucose, and 0.1% bovine serum albumin) to a final screening concentration of 67 μ M with 1% DMSO.

MOL 14068

fMLFF (4Pep blocked control) and fMLFK-FITC peptides were used at final concentrations of 150 and 1.5 nM, respectively. A starting cell stock of 10^7 cells/ml (in ADB) was diluted 1:3 in the final assay mixture ($\sim 3.3 \times 10^6$ cells/ml, 15 μ l total volume). This resulted in analysis of $\sim 2,500$ cells from each well when sampling at 40 wells/min (aspirated sample volume ~ 2 μ l) with HyperCyt[®].

The best flow cytometry sampling and analysis results are obtained with uniform cell suspensions. Significant cell settling may occur after 5-10 min in undisturbed wells (Ramirez et al., 2003). To minimize cell settling, test cells and fluorescent peptide ligand were added quickly (1-2 min) under automated control of a Titertek MAP-C liquid dispensing system. Specialized 96-well microplates were used (Greiner Imp@ct plate, Intermountain Scientific) that allowed retention of samples in wells (by surface tension) when the microplates were inverted. To maintain uniform cell suspensions during the two 4°C incubations, microplates were placed on a rotating cell suspension system device (in a refrigerator) that continuously rotated them between upright and inverted positions at 4 RPM (Ramirez et al., 2003). HyperCyt[®] sampling was completed in less than 3 min.

HyperCyt[®] The HyperCyt[®] platform (Kuckuck et al., 2001; Ramirez et al., 2003) interfaces a flow cytometer and autosampler. As the sampling probe of the autosampler moves from one well to the next of a multi-well microplate, a peristaltic pump sequentially aspirates sample particle suspensions from each well. Between wells, the continuously running pump draws a bubble of air into the sample line. This results in the generation of a tandem series of bubble-separated samples for delivery to the flow cytometer. Sample and bubble volumes are determined by the time that the autosampler probe is in a microplate well or above a well intaking air. We have validated cell-based high throughput endpoint assays for ligand binding, surface antigen expression, and immunophenotyping (Ramirez et al., 2003)

MOL 14068

Sample fluorescence was excited with a 488 nm laser in a BD Biosciences FacScan flow cytometer. The assay response data were measured in the FL1 green fluorescence emission channel (515-545 nm). The FL3 red fluorescence emission channel (>650 nm) was used for detection of Cytoflex L9 or L10 beads (Duke Scientific, Palo Alto, CA) that were added to a subset of wells to facilitate proper registration of flow cytometry data with source wells.

Some test compounds were inherently fluorescent when exposed to the 488 nm laser line, emitting fluorescence in the FL1 channel that compromised the assay's ability to detect effects of the compound upon binding of the green-fluorescent fMLFK-FITC ligand. To analyze such compounds, we modified the assay as previously described (Young et al., 2005) to use a hexapeptide FPR ligand (fNleLFNleYK, $K_d \sim 30$ nM) tagged with Alexa-633, a fluorescent probe excited by the red diode laser (635 nm excitation) of a FACS Calibur flow cytometer (BD Biosciences). Assay response data were then measured in the FL4 red fluorescence channel (>670 nm).

HyperCyt[®] data analysis. In the HyperCyt[®] platform, the air bubble-separated samples are delivered in a continuous stream to the flow cytometer. Likewise, the data are collected in a continuous stream, the accumulated data from all wells of a microplate representing a single data file. The time-resolved data, with periodic gaps corresponding to the passage of the sample-separating air bubbles, were analyzed by proprietary software (IDLeQuery). The program automatically detects the time-resolved data clusters, ensures that there are 96, and analyzes each to determine the MFI of bound peptide. These reduced data are automatically exported to a Microsoft Excel spreadsheet template that immediately calculates the assay quality control Z' factor and peptide binding inhibition percent for each well. Thus, comprehensive assay results are available within 1 to 2 min after assay plate sampling is completed. Because each sample consists of 2 μ l taken from a 15- μ l volume in each well, we routinely sampled and analyzed each plate twice and averaged the results in the Excel spreadsheet.

MOL 14068

K_i determinations. Ligand competition curves were fit by nonlinear least-squares regression using a one-site competition model with Prism[®] software (GraphPad Software, Inc., San Diego, CA) to determine the concentration of added competitor that inhibited fluorescent ligand binding by 50% (IC₅₀). FPR expression ranged from 100,000 to 400,000 receptors per cell in different assays as determined by comparison to standard curves generated with Fluorescein Reference Standard Microbeads (Bangs Laboratories, Fishers, IN). This corresponded to total FPR concentrations of 0.6 to 2.2 nM. To account for effects of ligand depletion at the higher receptor concentrations, K_i were calculated from the IC₅₀ by the method of Munson and Rodbard (Munson and Rodbard, 1988):

$$K_i = K_d \times [y_0 / (y_0 + 2)] + IC_{50} / \{1 + [p^* \times (y_0 + 2)] / [2 \times K_d \times (y_0 + 1)] + y_0\}$$

in which y₀ is the initial bound-to-free concentration ratio for the fluorescent ligand, p* is the added concentration of fluorescent ligand (1.5 nM) and K_d is the dissociation constant of the fluorescent ligand (3 nM).

Intracellular Ca²⁺ measurements. As previously described (Young et al., 2004), 10⁷ cells are resuspended in 10 ml of warm medium containing 200 nM Fluo4 acetoxymethyl ester (Molecular Probes, Eugene, OR) and incubated at 37°C for 30 minutes, with mixing every 10 minutes. After incubation, cells are washed twice by centrifugation and resuspended in complete HHB (110 mM NaCl, 30 mM HEPES, 10 mM KCL, 1mM MgCl₂, 10 mM glucose, and 0.1% (v/v) human serum albumin, and 1.5 mM CaCl₂). Cells are exposed to a range of compound concentrations to determine temporal (0-10 min) effects upon green Fluo4 fluorescence intensity of cells. A dose-response curve compares peak fluorescence intensities at each compound concentration.

To assess the ability of test compounds to block formylpeptide-induced Ca²⁺ responses, DeltaST cells (1 x 10⁶/ml) were incubated with and without the compound (100 μM final concentration) for 30 minutes on ice. Cells were

MOL 14068

warmed for 5 minutes, analyzed for 20 seconds using a FACScan™ flow cytometer to establish a baseline, then fML peptide (2Pep) was manually added to a final concentration of 50 nM and the analysis reinitiated. Cells were also stimulated by addition of ATP (1 μM final concentration) to evaluate compound effects upon detection of a Ca²⁺ response unrelated to FPR ligation.

Cell adhesion assays. Cell adhesion assays were performed essentially as previously described (Chigaev, 2003) to assess FPR-activated VLA4-dependent adhesion of DeltaST cells to VCAM-1 expressed on B78H1-VCAM1 cells. DeltaST cells were loaded with red-fluorescent Fura-Red and B78H1-VCAM1 cells with green-fluorescent 5-(and 6-)-carboxyfluorescein diacetate succinimidyl ester (CFSE) (both dyes from Molecular Probes) and maintained on ice until the experiment. 300 μl of DeltaST cells (1 x 10⁶ cells/ml) and 300 μl of B78H1-VCAM cells (3 x 10⁶ cells/ml) were incubated separately for 5 minutes at 37° C in the presence or absence of test compounds (100 μM final). Cells were then combined and analyzed in the flow cytometer during which time the cell suspension was continuously stirred at 300 rpm, 37°C with a magnetic microstirbar. After 90 s stirring to establish basal levels of cell adhesion, fMLFF (4PEP) was added to a final concentration of 10 nM and the analysis reinitiated to determine the increase in adhesion promoted by FPR ligation. Alternatively, to assess possible non-specific compound effects on adhesion, adhesion was activated by addition of MnCl₂ to a final concentration of 1 mM. DeltaST cells were resolved into two fractions in the flow cytometer: singlets (events that were uniformly red fluorescent) and conjugates (red/green co-fluorescent events containing red fluorescent DeltaST cells adherent to green fluorescent B78H1-VCAM1 cells). At each indicated time point the percent of adherent DeltaST cells was calculated as 100 x (number of conjugates)/(number of conjugates + number of singlets).

MOL 14068

Results

FPR Homology Model: Applicability and Limitations. Data from cross-linking and mutagenesis studies suggest that the FPR ligand binding site is located between the transmembrane helices, near the extracellular face of the membrane (Mills et al., 2000). The crystal structure of bovine rhodopsin (PDB code 1F88) was used as starting point for binding site modeling. The FPR and bovine rhodopsin sequences were aligned using T-Coffee package (Notredame et al., 2000), and manual corrections were made in order to avoid insertions/deletions in any alpha helix (Fig. 1). A homology model of the FPR seven transmembranar alpha-helices was then generated using SWISS-MODEL (Schwede et al., 2003), and further refined using the AMBER (Pearlman et al., 1995) force field (Fig 2 A and B). We assumed that no significant induced fit effects occur upon the binding and the receptor is rigid to a good approximation. The FPR homology model relied on primary sequence alignment tools (e.g., T-Coffee), which in themselves are good tools, but not reliable predictors for transmembrane domain relative positioning, helix kinks, etc. One must always be conscious of the “highly conserved residues” (Baldwin et al., 1997), which require manual insertions/deletions of residues that occur in the transmembrane domains. To illustrate such shortcomings, we had to manually modify torsion angles in the Arg205 side-chain, in order to force a salt-bridge interaction with Asp106; all other side-chains were geometry-optimized using AMBER. At this stage, the FPR homology model was used for the pharmacophore model construction.

Pharmacophore identification: Known agonists and antagonists were docked into the binding site of the model receptor using Autodock (Morris et al., 1998) (Fig. 2C), and a pharmacophore model was derived based on the docking results. The basis of the pharmacophore concept is that all ligands, regardless of chemical structure, bind in conformations that present similar steric and electrostatic features to the receptor – features that are recognized at the receptor site and are responsible for the biological activity (Güner, 2000). Built

MOL 14068

on Marshall's active analog approach (Marshall et al., 1979), pharmacophore methods require a computationally- or experimentally- derived ligand structure (or series) that can provide a reasonably good definition of bioactivity requirements (Beusen and Marshall, 2000). Most of the pharmacophore perception methods are incorporated in commercially available software and discussed in a book edited by Osman Güner (Güner, 2000).

To derive the antagonist pharmacophore model, we analyzed the following 4 ligands: thiazolyl-ureido-Phe-D-Leu-Phe-D-Leu-Phe (tF-D-LF-D-LF) (Dalpiaz et al., 2002); iso-butyloxycarbonyl-Met-Leu-Phe (iboc-MLP) (Derian et al., 1996); cyclosporin H (Loor et al., 2002); phenylbutazone (Nelson et al., 1981). These 4 ligands were docked, at the same time as 2 agonists, formyl-Met-Leu-Phe (fMLP) and formyl-Met-Met-Trp-Leu-Leu (fMMWLL), into the FPR homology model. The extracellular region of the 7 transmembranes was considered as the primary area of molecular recognition for antagonists, whereas the formylated moiety of the agonists (crucial for activity) was docked deeper into the transmembrane region. The top twenty conformers were selected for each of the 4 antagonists, and were used to derive the pharmacophore model. Fig. 2C shows a single low-energy conformation for the two agonists, fMLP and fMMWLL, and two antagonists, iboc-MLP and phenylbutazone. These results appear to indicate that the agonist- and antagonist-binding site overlap only in part.

Once the 80 conformers were overlapped into the FPR antagonist binding site, the final pharmacophore was generated after visual inspection, by identifying two acceptors and one hydrophobe point common to most of them (Fig. 2D). Distance tolerances between the two acceptors were 3-6 Å, and 4-7 Å and 5-7 Å, respectively, between the acceptors and the hydrophobe point. The key feature of this model was the addition of 23 exclusion spheres, i.e., sterically forbidden zones. While the pharmacophore as such could have been derived in the absence of the receptor, the addition of the exclusion spheres could not have been done without the FPR homology model. Thus, even though we consider

MOL 14068

this primarily a ligand-based virtual screening (LBVS) effort, we have used as much information about the target (FPR) as possible.

LBVS using the pharmacophore model: The LBVS query relied on a pharmacophore model (2 H-bond accepting centers, a hydrophobic area, and 23 excluded spheres) derived from receptor-induced ligand conformations, to which additional restrictions were added. The XCGen program (www.chemosoft.com) was used to perform a guided pharmacophore constrained structure-based screening strategy. XCGen performs a systematic grid search with some additions/corrections accounting for experimentally known stereochemical preferences of molecular fragments, molecular mechanics constraints and 3D pharmacophore geometry constraints. Exploration of conformers is therefore biased to those maximally matching the pharmacophore hypothesis, and the algorithm examines large numbers of putative ligand-receptor orientations, enabling the theoretical match of novel chemotypes.

The XCGen program generated conformations using standard stereochemical rules and molecular mechanics refinements. These conformers served as starting points for iterative modification of molecular geometry to improve the fit with the pharmacophore. Notably, XCGen did not find a pharmacophore match for over 100,000 compounds from the ChemDiv library. Quite likely, these compounds are not active against FPR. The best-fitting 4,234 compounds were selected for further HTFC screening.

HTFC screening of the FPR-focused compound collection. The 4,324 compounds identified by LBVS were subsequently screened in the HTFC FPR ligand binding assay. We found 95 hits (2.2%) that showed some inhibition in the primary assay, of which 52 (1.2%) were confirmed hits averaging $\geq 65\%$ inhibition and 30 (0.7%) had K_i s ranging from 1-32 μM (Table 1). These compounds represented 9 chemically distinct groups (Table 1, Groups A-F and H-J). There was one additional active compound from a tenth chemically distinct

MOL 14068

group (Group G), but the K_i was relatively large (49 μM) and it was not investigated further. Key characteristics of the chemical groups have been described elsewhere (Oprea et al., 2005).

Secondary screening for agonist activity. A hallmark of FPR agonist activity is a rise in intracellular Ca^{2+} concentration. A subset of 17 compounds with the lowest measured K_i ($\leq 10 \mu\text{M}$) was therefore evaluated for the ability to elicit intracellular Ca^{2+} responses in DeltaST cells. Compound 1910-5441 from Group A was identified to be a weak partial agonist. Partial agonist activity was indicated by elevation of intracellular Ca^{2+} concentration to a plateau level that was only ~75% of that elicited by the high-affinity agonist, fMLFF (Fig. 3). The effective concentration that elicited 50% of the maximal Ca^{2+} response (EC_{50}) was ~20 μM . By comparison, the EC_{50} of fMLFF was ~0.2 nM. Other Group A compounds also exhibited agonist activity when tested at concentrations of 50 μM or more (Fig. 3). This was commensurate with the higher K_i s of these compounds in ligand competition assays (4-10 μM) as compared to 1910-5441 (1 μM). Compounds from the other groups were inactive in Ca^{2+} response assays at concentrations up to 200 μM (data not shown). Therefore compounds from all but Group A were antagonists, in concert with predictions of the computational model used for virtual screening.

Secondary screening to confirm antagonist activity. To confirm that compounds exclusive of Group A were antagonists, representative compounds from each group were assessed for the ability to inhibit Ca^{2+} responses induced by an FPR agonist. In the absence of test compounds the peptide fML (2Pep) promoted a rapid increase in Fluo4 fluorescence intensity, indicative of elevated intracellular Ca^{2+} , that peaked within 5-10 s of 2Pep addition (Fig 4, A-C). This response was abrogated in the presence of representative compounds from Groups D, E and H (Fig. 4, A-C). By contrast, the cell Ca^{2+} response to addition of ATP was unaffected by the presence of any of the compounds (Fig. 4, A-C), an indication that the 2Pep results were not attributable to nonspecific effects of the

MOL 14068

compounds upon Fluo4 fluorescence or Ca^{2+} responses triggered by an FPR-independent pathway. Similar results were obtained with compounds from Groups B, C, F, I and J (Figs. 6 and 7 in supplementary material available online).

To further verify antagonist activity, compounds were tested for the additional ability to block cell adhesion responses stimulated by FPR ligation. Consistent with results of previous studies (Chigaev, 2003), ligation of FPR with fMLFF (4Pep) promoted an increase in VLA4-dependent adhesion of DeltaST cells to human VCAM-1 expressed on B78H1-VCAM1 cells (Fig 4, D-F). The adhesion response to 4Pep was blocked in the presence of compounds from Groups D,E and H (Fig. 4, D-F). MnCl_2 , which promotes VLA4/VCAM-1 adhesion by an alternative FPR-independent mechanism, triggered an adhesion response in the presence of compounds that was at most only marginally less than what was observed in their absence (Fig. 4, D-F). Adhesion responses to both 4Pep and MnCl_2 were mediated by VLA4, as indicated by inhibition of adhesion in the presence of a peptide that directly blocked the VLA4 binding site (Chigaev, 2003 and data not shown). Thus, these compounds as well as representative compounds from the five other putative antagonist groups (data not shown) exhibited antagonist activity for FPR-dependent adhesion responses.

Discussion

In this paper, we illustrate how ligand-based virtual screening can be combined with high-throughput physical screening in order to identify novel ligands for a target with unknown structure. We considered this approach in particular since the FPR homology model(s), while useful in a qualitative sense, represents an unquantifiable departure from reality. However, this limitation proved useful in generating volume restrictions for the pharmacophore model (Fig. 2D). Data from cross-linking and mutagenesis studies suggest that the FPR ligand binding site is located between the transmembrane helices, near the extracellular face of

MOL 14068

the membrane (Mills et al., 2000). Several weak micromolar binders (phenylbutazone and related pyrazolidinedione drugs) and strong nanomolar binders: cyclosporins and formylpeptide derivatives had been previously described (Bae et al., 2003; Dalpiaz et al., 2002). This information was integrated to generate a novel combined FPR model / pharmacophore model which we then used as a basis for virtual screening to identify a highly focused subset of compounds likely to contain FPR antagonists.

In our previous physical screening of the Prestwick Compound Library (880 molecules) with the HyperCyt[®] platform we detected one true hit - a phenylbutazone derivative with $K_i \sim 14 \mu\text{M}$, and one false positive with non-specific activity (Young et al., 2005). This represented a hit frequency of 0.1%, typical of a random collection of compound structures. In the present study integration of virtual screening with HyperCyt[®] screening resulted in 52 confirmed hits for a 12-fold improvement in hit frequency. After secondary dose-response studies, we found 17 of the 52 (33%) to have $K_i \leq 10 \mu\text{M}$. The active compounds represented 9 distinct chemotype groups (Table 1). Compounds from 8 groups were confirmed to be antagonists of FPR-dependent Ca^{2+} and cell adhesion responses (Fig. 4). Compounds from the remaining group (Group A) were shown to act as partial FPR agonists in Ca^{2+} response assays (Fig. 3). The active compounds match within 1 Å tolerance the pharmacophore shown in Figure 2D (data not shown). Two examples, from chemotype groups A (1495-0037; $K_i = 10 \mu\text{M}$) and E (1682-2108; $K_i = 6 \mu\text{M}$), are depicted in Figure 5. Although the pharmacophore has the same orientation in the illustration, it is apparent that the two molecules overlap well at the pharmacophore feature level only, i.e., other features are not assigned the same orientation. Given the level of bioactivity (1-10 μM) of these compounds, further attempts to improve the overlap between these molecules are not necessary, since the precision of such calculations is not warranted by the level of bioactivity.

MOL 14068

This and previous studies (Young et al., 2005) demonstrate the HyperCyt[®] platform for HTFC screening to be a robust, sensitive and highly quantitative method with which to screen lead compound libraries in a 96-well format. This screening approach allows high throughput ligand-binding assays to be performed in a no-wash homogeneous format that would not be feasible with conventional fluorescence plate-readers, a reflection of the superior ability of the flow cytometer to distinguish bound ligand in the presence of unbound fluorescent ligand. Moreover, HyperCyt[®] HTFC is presently amenable to miniaturization down to total assay volumes as small as 8 μ l/well, from which sample volumes of 2 μ L are routinely sufficient for ligand binding analysis, as demonstrated in the present study. It is also noteworthy that this physical screening approach is capable of detecting compounds with K_i s up to the tens-of- μ M range, minimizing the likelihood of missing novel lead compounds that might be amenable to chemical optimization.

All FPR hits were categorized by chemotype: The 9 families having 52 confirmed hits were prioritized using an empirical evaluation scheme, described elsewhere (Oprea et al., 2005). Briefly, we awarded negative scores whenever the chemotype was already present in publications or patents, or whenever it tested positive in toxicity-related experiments. Positive scores were awarded for higher FPR activity, for testing negative in toxicity-related literature, and for good overlap when profiled against drug-related properties (Oprea, 2000). Based on this analysis, three chemotypes have been selected for further experiments.

In this study, a combination of virtual and physical screening enabled discovery of a series of chemotypes with higher FPR activity than any previously reported non-cyclosporin drugs. Thus, in the absence of precise 3D structural information for a GPCR, modeling on the basis of rhodopsin homology and appropriate pharmacophore selection can significantly augment screening efficiency for detection of active compounds.

MOL 14068

Acknowledgements

Technical and instrument support was provided by the Shared Flow Cytometry Resource in the University of New Mexico Cancer Research and Treatment Center. Software and hardware support were provided by the Division of Biocomputing at the University of New Mexico Health Sciences Center.

MOL 14068

References

- Bae YS, Song JY, Kim Y, He R, Ye RD, Kwak JY, Suh PG and Ryu SH (2003) Differential activation of formyl peptide receptor signaling by peptide ligands. *Mol Pharmacol* **64**:841-7.
- Baldwin JM, Schertler GF and Unger VM (1997) An alpha-carbon template for the transmembrane helices in the rhodopsin family of G-protein-coupled receptors. *J Mol Biol* **272**:144-64.
- Beusen DD and Marshall GR (2000) Pharmacophore definition using the active analog approach., in *Pharmacophore Perception, Development and Use in Drug Design* (Guner O ed) pp 21-45, International University Line, La Jolla.
- Carp H (1982) Mitochondrial N-formylmethionyl proteins as chemoattractants for neutrophils. *J Exp Med* **155**:264-75.
- Chigaev A, Zwartz G, Graves SW, Dwyer DC, Tsuji H, Foutz TD, Edwards BS, Prossnitz ER, Larson RS, and Sklar LA (2003). Alpha4beta1 integrin affinity changes govern cell adhesion. *J Biol Chem* **278**: 38174-38182.
- Dalpiaz A, Ferretti ME, Vertuani G, Traniello S, Scatturin A and Spisani S (2002) C- and N-terminal residue effect on peptide derivatives' antagonism toward the formyl-peptide receptor. *Eur J Pharmacol* **436**:187-96.
- Derian CK, Solomon HF, Higgins JD, 3rd, Beblavy MJ, Santulli RJ, Bridger GJ, Pike MC, Kroon DJ and Fischman AJ (1996) Selective inhibition of N-formylpeptide-induced neutrophil activation by carbamate-modified peptide analogues. *Biochemistry* **35**:1265-9.
- Gao JL, Lee EJ and Murphy PM (1999) Impaired antibacterial host defense in mice lacking the N-formylpeptide receptor. *J Exp Med* **189**:657-62.
- Güner O (ed) (2000) *Pharmacophore Perception, Development and Use in Drug Design*. International University Line, La Jolla.
- He R, Sang H and Ye RD (2003) Serum amyloid A induces IL-8 secretion through a G protein-coupled receptor, FPRL1/LXA4R. *Blood* **101**:1572-81.

MOL 14068

- Key TA, Foutz TD, Gurevich VV, Sklar LA and Prossnitz ER (2003) N-formyl peptide receptor phosphorylation domains differentially regulate arrestin and agonist affinity. *J Biol Chem* **278**:4041-7.
- Kuckuck FW, Edwards BS and Sklar LA (2001) High throughput flow cytometry. *Cytometry* **44**:83-90.
- Le Y, Jiang S, Hu J, Gong W, Su S, Dunlop NM, Shen W, Li B and Ming Wang J (2000) N36, a synthetic N-terminal heptad repeat domain of the HIV-1 envelope protein gp41, is an activator of human phagocytes. *Clin Immunol* **96**:236-42.
- Le Y, Murphy PM and Wang JM (2002) Formyl-peptide receptors revisited. *Trends Immunol* **23**:541-8.
- Le Y, Oppenheim JJ and Wang JM (2001) Pleiotropic roles of formyl peptide receptors. *Cytokine Growth Factor Rev* **12**:91-105.
- Loor F, Tiberghien F, Wenandy T, Didier A and Traber R (2002) Cyclosporins: structure-activity relationships for the inhibition of the human FPR1 formylpeptide receptor. *J Med Chem* **45**:4613-28.
- Marasco WA, Phan SH, Krutzsch H, Showell HJ, Feltner DE, Nairn R, Becker EL and Ward PA (1984) Purification and identification of formyl-methionyl-leucyl-phenylalanine as the major peptide neutrophil chemotactic factor produced by *Escherichia coli*. *J Biol Chem* **259**:5430-9.
- Marshall GR, Barry CD, Bosshard HE, Dammkoehler RA and Dunn DA (1979) The conformational parameter in drug design: the active analog approach., in *American Chemical Society Symposium Series, Vol. 112* (Olson EC and Christofferson RE eds) pp 205-226, American Chemical Society, Washington DC.
- Mills JS, Miettinen HM, Cummings D and Jesaitis AJ (2000) Characterization of the binding site on the formyl peptide receptor using three receptor mutants and analogs of Met-Leu-Phe and Met-Met-Trp-Leu-Leu. *J Biol Chem* **275**:39012-7.
- Morris GM, Goodsell DS, Halliday RS, Huey R, Hart WE, Belew RK and Olsen AJ (1998) Automated docking using a Lamarkian genetic algorithm and an

MOL 14068

- empirical binding free energy function. *J. Computational Chem* **19**:1639-1662.
- Munson PJ and Rodbard D (1988) An exact correction to the "Cheng-Prusoff" correction. *J Recept Res* **8**:533-46.
- Murphy PM (1994) The molecular biology of leukocyte chemoattractant receptors. *Annu Rev Immunol* **12**:593-633.
- Nelson RD, Gracyk JM, Fiegel VD, Herron MJ and Chenoweth DE (1981) Chemotactic deactivation of human neutrophils: protective influence of phenylbutazone. *Blood* **58**:752-8.
- Notredame C, Higgins DG and Heringa J (2000) T-Coffee: A novel method for fast and accurate multiple sequence alignment. *J Mol Biol* **302**:205-17.
- Olah MM, Bologa CG and Oprea TI (2004) Strategies for compound selection. *Curr Drug Discov Technol* **1**:211-220.
- Oppenheim JJ, Zachariae CO, Mukaida N and Matsushima K (1991) Properties of the novel proinflammatory supergene "intercrine" cytokine family. *Annu Rev Immunol* **9**:617-48.
- Oprea TI (2000) Property distribution of drug-related chemical databases. *J Comput Aided Mol Des* **14**:251-64.
- Oprea TI, Bologa C, Edwards BS, Prossnitz E and Sklar LA (2005) Post-HTS analysis: an empirical prioritization scheme. *J Biomol Screen*, in press.
- Pearlman DA, Case DA, Caldwell CW, Ross WS, Cheatham TE, Debolt S, Ferguson D, Seibel G and Kollman P (1995) "Amber", a package of computer programs for applying molecular mechanics, normal mode analysis, molecular dynamics and free energy calculations to simulate the structural and energetic properties of molecules. *Comput Physics Commun* **91**:1-42.
- Prossnitz ER (1997) Desensitization of N-formylpeptide receptor-mediated activation is dependent upon receptor phosphorylation. *J Biol Chem* **272**:15213-9.

MOL 14068

- Ramirez S, Aiken CT, Andrzejewski B, Sklar LA and Edwards BS (2003) High-throughput flow cytometry: Validation in microvolume bioassays. *Cytometry* **53A**:55-65.
- Schiffmann E, Corcoran BA and Wahl SM (1975) N-formylmethionyl peptides as chemoattractants for leucocytes. *Proc Natl Acad Sci U S A* **72**:1059-62.
- Schwede T, Kopp J, Guex N and Peitsch MC (2003) SWISS-MODEL: An automated protein homology-modeling server. *Nucleic Acids Res* **31**:3381-5.
- Su SB, Gao J, Gong W, Dunlop NM, Murphy PM, Oppenheim JJ and Wang JM (1999) T21/DP107, A synthetic leucine zipper-like domain of the HIV-1 envelope gp41, attracts and activates human phagocytes by using G-protein-coupled formyl peptide receptors. *J Immunol* **162**:5924-30.
- Tiffany HL, Lavigne MC, Cui YH, Wang JM, Leto TL, Gao JL and Murphy PM (2001) Amyloid-beta induces chemotaxis and oxidant stress by acting at formylpeptide receptor 2, a G protein-coupled receptor expressed in phagocytes and brain. *J Biol Chem* **276**:23645-52.
- VanCompernelle SE, Clark KL, Rummel KA and Todd SC (2003) Expression and function of formyl peptide receptors on human fibroblast cells. *J Immunol* **171**:2050-6.
- Walther A, Riehemann K and Gerke V (2000) A novel ligand of the formyl peptide receptor: annexin I regulates neutrophil extravasation by interacting with the FPR. *Mol Cell* **5**:831-40.
- Young SM, Curry MS, Ransom JT, Ballesteros JA, Prossnitz ER, Sklar LA and Edwards BS (2004) High-throughput microfluidic mixing and multiparametric cell sorting for bioactive compound screening. *J Biomol Screen* **9**:103-11.
- Young SM, Bologna C, Prossnitz E, Oprea TI, Sklar LA and Edwards BS (2005) High throughput screening with HyperCyt flow cytometry to detect small molecule formylpeptide receptor ligands. *J Biomol Screen* **10**:374-382..

MOL 14068

Zhang JH, Chung TD and Oldenburg KR (1999) A Simple Statistical Parameter for Use in Evaluation and Validation of High Throughput Screening Assays. *J Biomol Screen* **4**:67-73.

MOL 14068

Footnotes

This work was supported in part by National Institutes of Health grants AI48517, R24-GM-60799 (now EB00264), R24-CA88339, by the University of New Mexico Cancer Research and Treatment Center, and by New Mexico Tobacco Settlement funds for Biocomputing.

Address reprint requests to: Tudor I. Oprea, Division of Biocomputing, MSC11 6145, UNM HSC, Albuquerque NM 87131; E-mail, TOprea@salud.unm.edu

MOL 14068

Figure Legends

Figure 1. The sequence alignment of the formyl-peptide receptor with bovine rhodopsin (PDB code: 1F88). Red - alpha-helices; underline - highly conserved residues in the GPCR family of receptors[*4]; * - identical residues; . - similar residues.

Figure 2. Computational modeling of the FPR and FPR ligands. Illustrated at top are hypothesized structures in the FPR homology model for (A) trans-membrane helices only and (B) residues 1-337 of the FPR. C. Docking of known agonists and antagonists into the binding site of the model receptor. Illustrated are binding modes of two agonists (red) and two antagonists (blue) as predicted by Autodock. D. Three-points pharmacophore model for FPR antagonists. Analysis of 80 conformers (20 from each of 2 agonists and 2 antagonists) identified two acceptors (red) and one hydrophobe point (blue) common to most. Distance tolerances between the acceptors and the hydrophobe point, and between the two acceptors were 5-7 Å, 3-6 Å, and 4-7 Å, respectively. A key feature of this model was the addition of 23 exclusion spheres, i.e., sterically forbidden zones (white lattice structures).

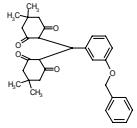
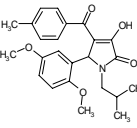
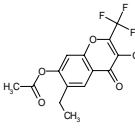
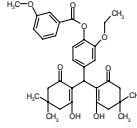
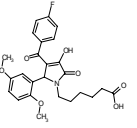
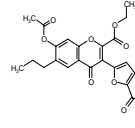
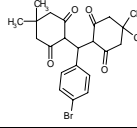
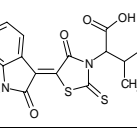
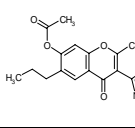
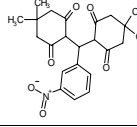
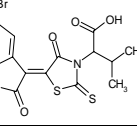
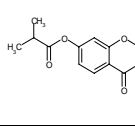
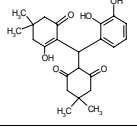
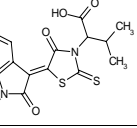
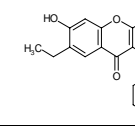
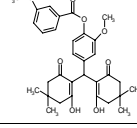
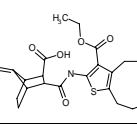
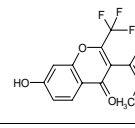
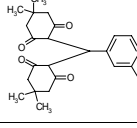
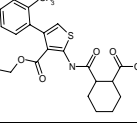
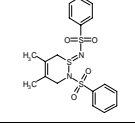
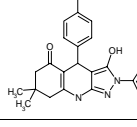
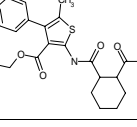
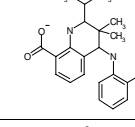
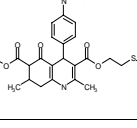
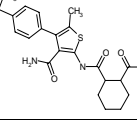
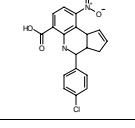
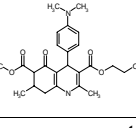
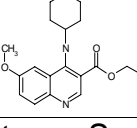
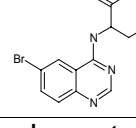
Figure 3. Agonist activity of Group A compounds. Group A compounds were compared with a high-affinity FPR agonist (4Pep, circles) for the ability to elicit elevation of intracellular Ca^{2+} ion concentration in DeltaST cells. Compound 1910-5441 (upright triangles) had an EC_{50} of $\sim 20 \mu\text{M}$ and a plateau response $\sim 75\%$ of that elicited by 4Pep. Compounds 5547-0066 (inverted triangles), 1495-0037 (squares) and 1495-0040 (diamonds) also elicited responses at higher concentrations, but full dose response curves could not be generated due to non-specific effects of DMSO solvent at compound concentrations $> 200 \mu\text{M}$. None of these compounds promoted Ca^{2+} responses in parental U937 cells that lacked FPR (data not shown).

MOL 14068

Figure 4. Confirmation of antagonist activity in Ca^{2+} response and cell adhesion assays. DeltaST cells loaded with the fluorescent intracellular Ca^{2+} probe Fluo4 were pre-incubated in the absence (open symbols) or presence (filled symbols or dashed line) of active compounds (100 μM final concentration), then analyzed in the flow cytometer to assess temporal fluorescence intensity responses to addition of 50 nM formylpeptide fML (2Pep, triangles), 1 μM ATP (diamonds), or no stimulus (dashed line). Results are representative of 2 or more assays performed with compounds from Groups D (panel A), E (panel B), and H (panel C). DeltaST cells labeled with red-fluorescent FuraRed were combined in stirred suspensions with B78H1-VCAM1 cells labeled with green-fluorescent CFSE to assess VLA4-dependent adhesion of DeltaST cells to B78H1-VCAM1 cells in the flow cytometer. Cells preincubated in the absence or presence of compounds (100 μM final concentration) are indicated as in the Ca^{2+} response assays. After 90 s of preliminary analysis, 10 nM fMLFF (4Pep, triangles), 1 mM MnCl_2 (diamonds), or no stimulus (dashed and solid lines without symbols) was added and subsequent effects upon the % of adherent DeltaST cells measured. Illustrated are results obtained with representative compounds from Groups D (panel D), E (panel E) and H (panel F). Compounds from Groups B (6359-0291), C (C119-0054), F (6049-0473), I (4393-0018), and J (4358-1479) were also tested in both Ca^{2+} response and cell adhesion assays with similar results (Figures 6 and 7 in supplementary material available online).

Figure 5. Pharmacophore matching for two confirmed hits from the A (top) and E (bottom) chemotype families.

Table 1. Chemical Diversity library compounds with FPR ligand binding activity.

Compound	Structure	Compound	Structure	Compound	Structure
Group A 1910-5441 Ki 1 μ M		Group D 4622-8438 Ki 4 μ M		Group H 3335-0327 Ki 2 μ M	
Group A 5547-0066 Ki 4 μ M		Group D 4393-0018 Ki 12 μ M		Group H 2188-3754 Ki 6 μ M	
Group A 1495-0037 Ki 10 μ M		Group E 1682-2106 Ki 4 μ M		Group H 2188-3197 Ki 10 μ M	
Group A 1495-0040 Ki 10 μ M		Group E 1682-2108 Ki 6 μ M		Group H 3230-2889 Ki 10 μ M	
Group A 5145-0561 Ki 21 μ M		Group E 3331-1295 Ki 7 μ M		Group H 3333-4944 Ki 12 μ M	
Group A 5547-0065 Ki 22 μ M		Group F 6049-0473 Ki 8 μ M		Group H 3335-0384 Ki 22 μ M	
Group A 1910-5443 Ki 32 μ M		Group F 6049-2423 Ki 11 μ M		Group I 2293-2337 Ki 3 μ M	
Group B 6359-0291 Ki 4 μ M		Group F 6049-2738 Ki 21 μ M		Group I 3454-2064 Ki 12 μ M	
Group C C119-0054 Ki 7 μ M		Group F 6049-2563 Ki 28 μ M		Group I 2448-0030 Ki 16 μ M	
Group C C142-0035 Ki 10 μ M		Group J 4358-1479 Ki 21 μ M		Group I 4300-0286 Ki 26 μ M	

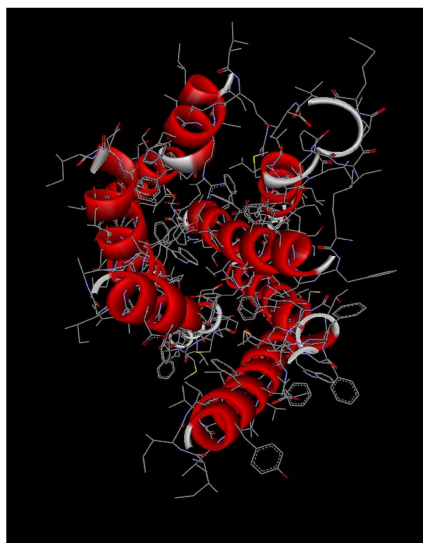
* Each group represents a distinct chemotype. Specific chemotype characteristics of each group are described elsewhere (Oprea et al., 2005).

Figure 1

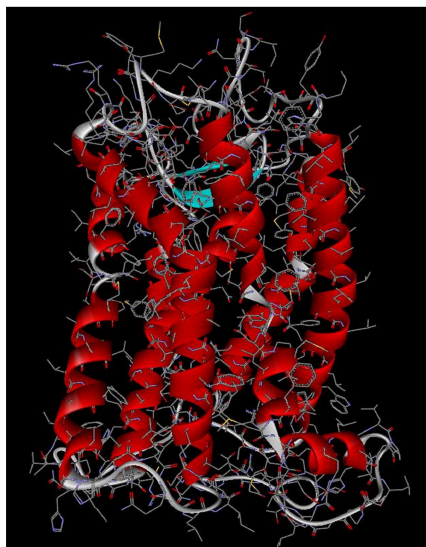
FPR	1	METN	SSLPTNI	---	SGGTPAVSAG	Y	----	LFLDI	ITYLVFAVTF
1f88A	1	MNGT	--EGPN	FYVPFSNKTG	VVRSPFEAPQ	YYLAEP	WQFS	MLAAYMFLLI	
			*	.*	.	.	*	.	.
FPR	38	VLGVLGNGLV	IWVAGFR-MT	HTVTTISYLN	LAVADFCFTS	TLPFFMVRKA			
1f88A	49	MLGFPINFLT	LYVTVQ	HKKL	RTPLNYILLN	LAVADLFMVF	GGFTTTLYTS		
		.*	*	*	.	*	.	.	.
FPR	87	MGGHWPFGWF	LCKFLFTIVD	INLFGSVFLI	A LIALDRCVC	VLHPVWTQNH			
1f88A	99	LHG YFVFGPT	GCNLEGGFAT	LGGEIALWSL	VVLAIERVYV	VCKPM--SNF			
		.	*	**	*
FPR	137	RTV -SLAKKV	IIGP WVMALL	LTL PVIIRVT	TVPGKTGTVA	CTFNFSPWTN			
1f88A	147	RFGE NHAIMG	VAFTWVMALA	CAAPPLVG	WS RYIPEGMQCS	CGIDYYTPHE			
		*	.	*
FPR	186	DPKERINVAV	AML TVRGIIR	FIIG FSAPMS	IVAVS YGLIA	TKIHKQGLI -			
1f88A	197	ET -----	-NNE SFVIYM	FVVFHIIPLI	VIFFCYGQLV	FTVKEAASA			
		.	.	*	*	.	.	*	.
FPR	235	----KSSRPL	RVL SFVAAA	F FLCWSPYQVV	ALIATV RIRE	LLQGM YKEIG			
1f88A	242	TTQKAE KEVT	RMVIIMVIAF	LICWLPYAGV	AFYIFT H---	---QGSDFGP			
			*	.	.	.	*	*	.
FPR	281	IAVDVTSALA	FFNSCL NPML	YVFMGQDFRE	RLIHALPASL	ERALTEDSTQ			
1f88A	286	IFMTIPAFFA	KTSAVYNPVI	YIM MNKQFRN	CMVTTLCCGK	NPSTTVSKTE			
		*	.	.	.	*	.	*	.
FPR	331	TSDTATN							
1f88A	342	TSQVAPA -							
		**	.	*					

Figure 2

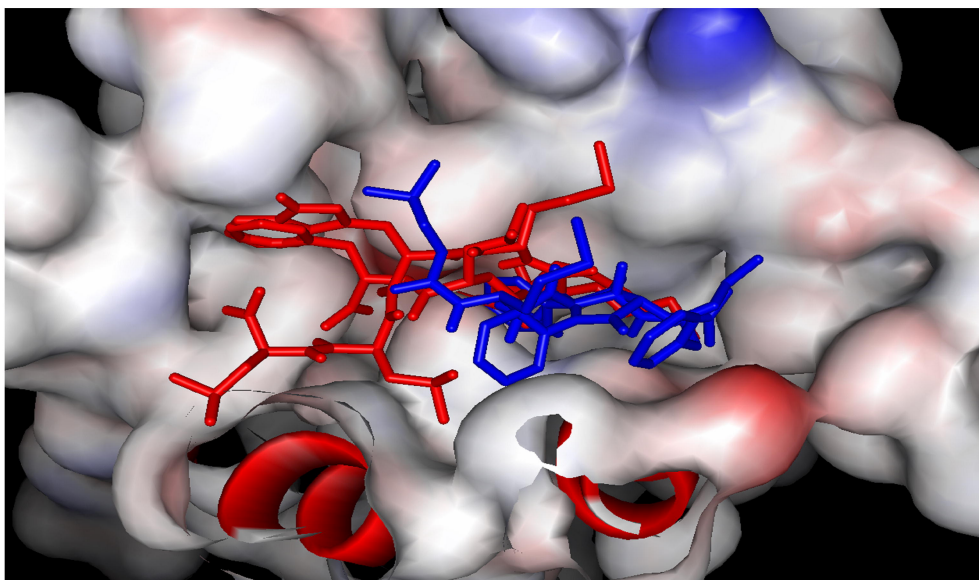
A



B



C



D

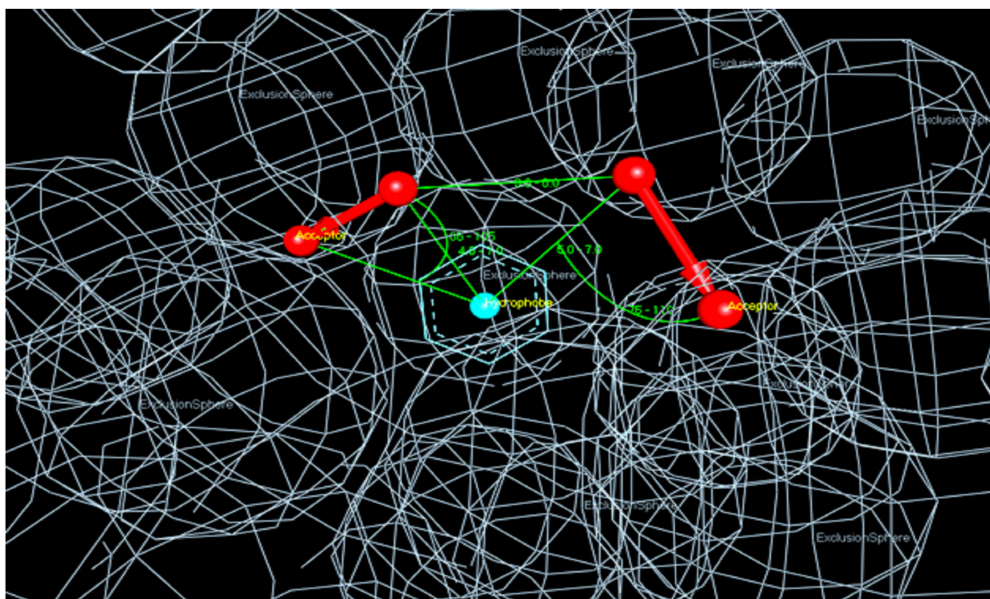


Figure 3

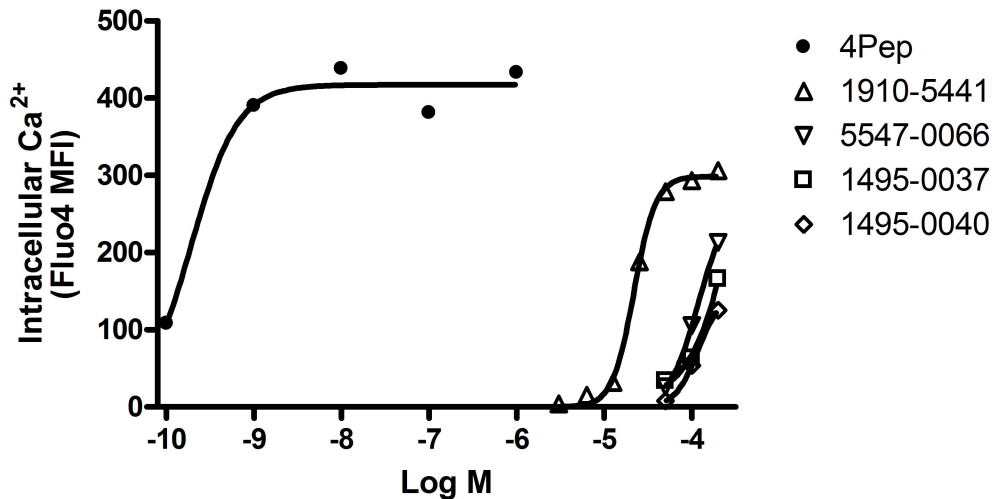
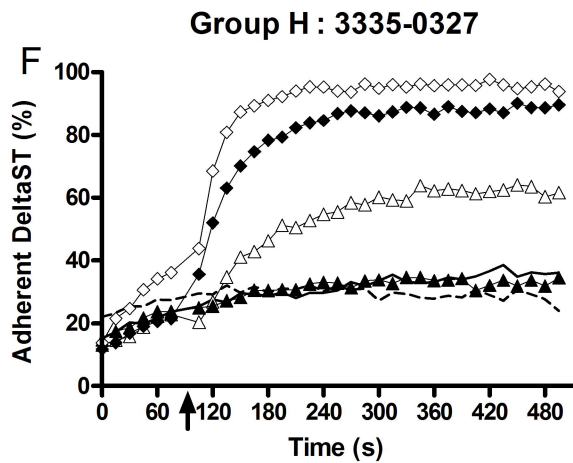
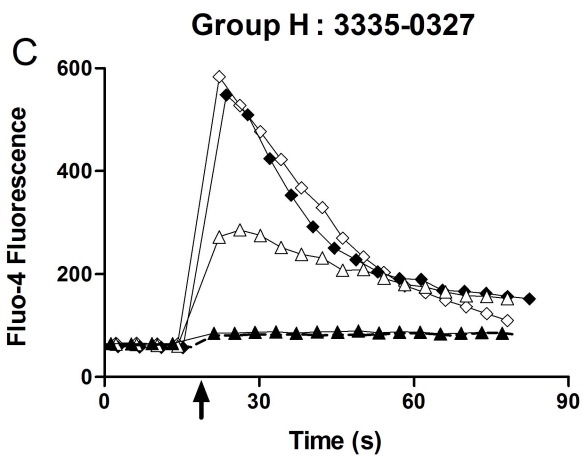
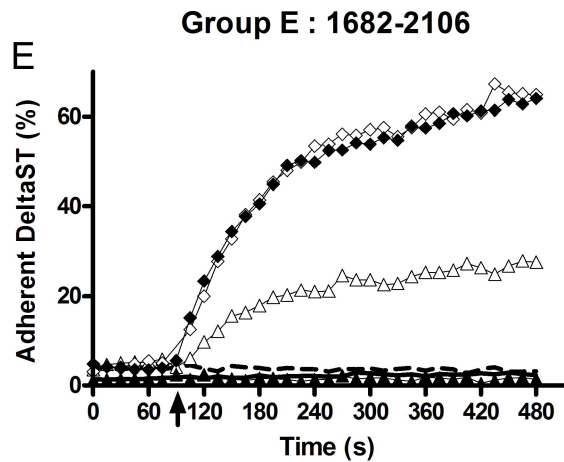
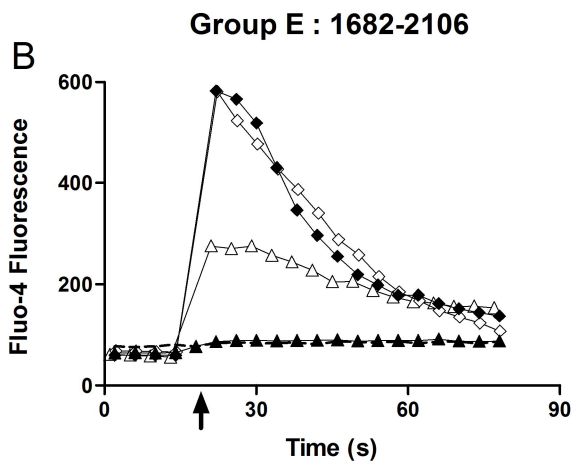
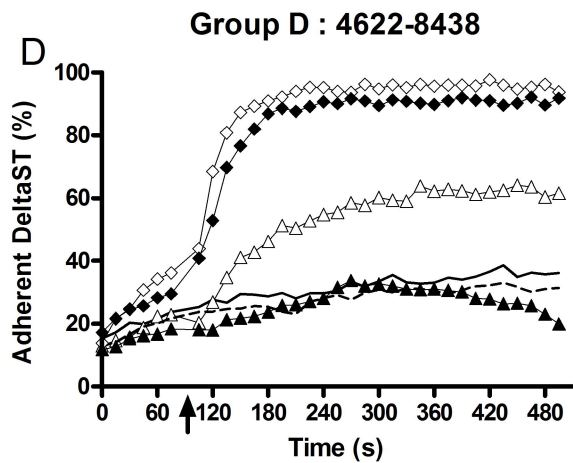
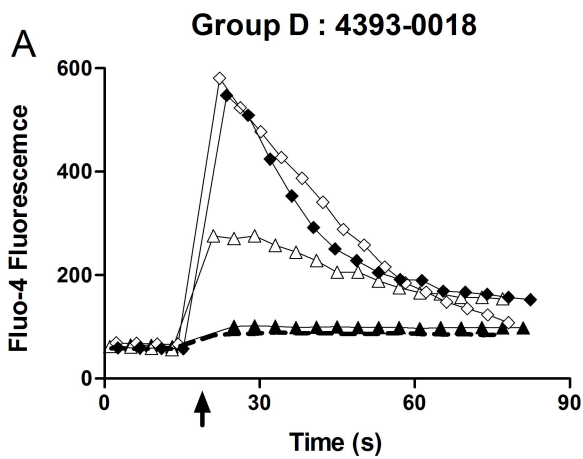


Figure 4

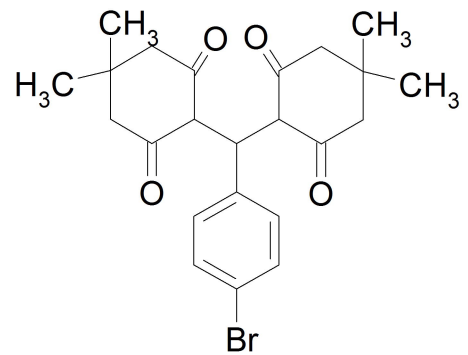
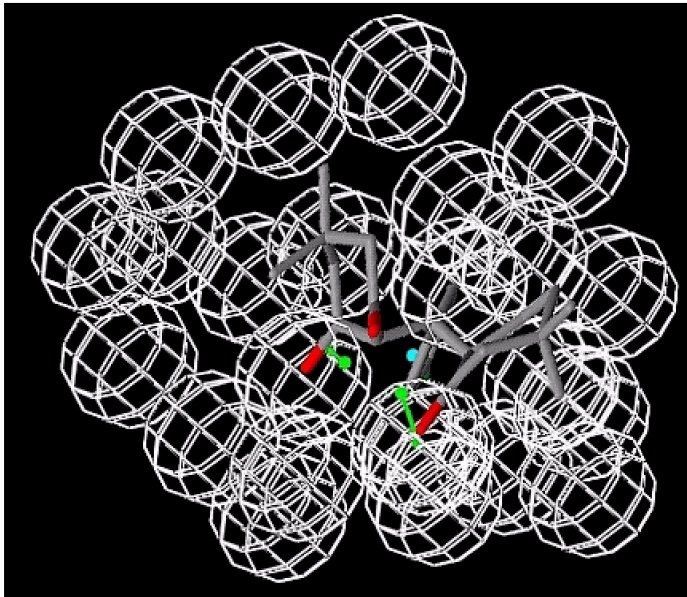


--- Compound Only
 -△- 2Pep Only ▲- 2Pep + Compound
 -◇- ATP Only ◆- ATP + Compound

— Untreated --- Compound Only
 -△- 4Pep Only ▲- 4Pep + Compound
 -◇- Mn⁺⁺ Only ◆- Mn⁺⁺ + Compound

Figure 5

A



B

